Flow and Heat Transfer Measurements in a Pseudo-Shock Region with Surface Cooling

Robert F. Cuffel* and Lloyd H. Back†
Jet Propulsion Lab., California Institute of Technology, Pasadena, Calif.

An experimental investigation was conducted to acquire information on the flow structure, mean flowfield, and temperature distributions in a pseudo-shock region in a supersonic diffuser with surface cooling. The Mach number upstream was 2.9, and the wall to stagnation temperature ratio was 0.44. A Mach-disk-like shock wave emanated from the thin separated flow region near the beginning of the compression region, and reattachment occurred one diameter downstream so that the flow was not separated over most of the pseudo-shock region. The flow compression was a shock-free, predominantly viscous process. Along the pseudo-shock region the measured heat-transfer coefficient increased approximately as the 0.8 power of the measured wall static pressure. The estimated wall shear stress increased downstream of flow attachment, but was still considerably less than the upstream value.

Nomenclature

c_f = friction coefficient $(c_f/2) = (\tau_w/\rho_e u_e^2)$
c_p = specific heat at constant pressure
D = diffuser diameter
h = heat transfer coefficient
H = enthalpy
M = Mach number
p = static pressure
p_t = total (stagnation) pressure
q_w = wall heat flux
r = radial distance
r_w = diffuser radius
S = shock wave
St = Stanton number $(h/\rho_e u_e)$
T = static temperature
T_t = total (stagnation) temperature
T_t^+ = dimensionless temperature, $(T_t - T_w)/(q_w/\rho_w/u_\tau c_{p_w})$
u = velocity component parallel to wall
u^+ = dimensionless velocity, u/u_τ
u_τ = friction velocity $(\tau_w/\rho_w)^{1/2}$
y = distance normal to wall
y^+ = dimensionless normal distance $(\rho_w u_\tau y/\mu_w)$
z = axial distance
α = frictional heating parameter $(u_\tau^2/2c_{p_w} T_w)$
β = heat transfer parameter $(q_w/T_w \rho_w u_\tau c_{p_w})$
δ = velocity boundary-layer thickness
δ^* = displacement thickness
Δ = thermal boundary-layer thickness
γ = specific heat ratio
Θ = momentum thickness
μ = viscosity
ρ = density
τ_w = wall shear stress
ϕ = energy thickness
ψ = stream function

Subscripts

0 = in duct upstream of nozzle
1 = upstream of pseudo-shock region at probe position 1
2 = at probe position 2
a = atmospheric condition
e = condition at edge of boundary layer
t = stagnation condition
w = wall condition

Received Feb. 4, 1976; revision received July 1, 1976. This work presents the results of one phase of research carried out in the Energy and Materials Research Section of the Jet Propulsion Laboratory, California Institute of Technology, under Contract NAS7-100, sponsored by the National Aeronautics and Space Administration.

Index categories: Shock Waves and Detonations; Boundary Layers and Convective Heat Transfer – Turbulent; Nozzle and Channel Flow.

*Member Technical Staff. Member AIAA.
†Member Technical Staff. Associate Fellow AIAA.

Introduction

SUPERSONIC exhaust diffusers are frequently employed in ground level tests of rocket engines[1] to reduce the ambient pressures sufficiently below atmospheric pressure to insure that flow separation will not occur in the nozzle. In this mode of operation a strong compression process occurs in the diffuser that has been referred to as pseudo-shock.[2] In the pseudo-shock region vigorous turbulent momentum exchange is believed to take place, but there is little quantitative experimental data on the flowfield and temperature distributions, especially with surface cooling. Recent pitot pressure surveys and wall shear stress measurements in a constant diameter duct[3,4] with an essentially adiabatic wall have revealed a multiple oblique shock wave pattern in the core flow with boundary-layer separation occurring throughout the compression region.

The present investigation was conducted using radial surveys with various probes (i.e., pitot, static pressure, and thermocouple probes) at a number of axial stations to provide information on the flow structure, mean flowfield, and temperature distributions in a pseudo-shock region with surface cooling. Information was obtained on the wall heat transfer accompanying the compression process and on its relative magnitude compared to single shock wave-turbulent boundary-layer interactions. Heat-transfer rates are important in establishing cooling requirements in diffusers and in inlets and combustor regions of hypersonic vehicles, especially since shock wave-turbulent boundary-layer interactions cause higher heating rates to occur. The wall shear stress was also estimated from the boundary-layer measurements obtained with relatively small probes that extended into the viscous sublayer upstream and within the pseudo-shock region.

Experimental Apparatus

The cooled system (Fig. 1) consisted of three sections: 1) a short subsonic duct 12.7 cm in diameter and 1.4 diam long, 2) a supersonic nozzle with convergent and divergent half-angles of 10° and a circular arc throat region with a 4.04 cm diam throat, and 3) a diffuser with a relatively long second throat, 10.8 cm in diameter, and 11 diam long. Prior to entering this

system, the air was compressed, heated, and accelerated; forming a thin, tripped, velocity boundary layer at the duct inlet. Prior to heating the air by the internal combustion of methanol, the air mass flow rate was measured with an orifice, and the methanol flow rate was measured with a rotameter. The total gas flow rate was 1.18 kg/sec. Thermodynamic properties and flow variables were calculated for the products of combustion, but transport properties were calculated for air since the methanol-to-air mass flow rate was only 3.1%.

The stagnation conditions, $T_{t0} = 835°$K and $p_{t0} = 6.55$ atm, were measured in the upstream cooled duct section. The pitot tube and three thermocouples were spaced 90° apart circumferentially. The pitot tube was on the centerline, while the thermocouples were 2.5 cm radially from it. A boundary-layer survey indicated that the flow was turbulent.

The entire cooled system was instrumented with semilocal circumferential coolant passages, and wall static pressure taps. The measurements reported herein were made in the latter half of the constant diameter section of the diffuser where the strong compression process referred to as a pseudo-shock occurred. The diffuser throat section was composed of several interchangeable sections and rings. The order of these was changed to place the probe ring at various axial locations without changing the length of the diffuser. The warm water circulating in the coolant passages maintained the wall to total gas temperature ratio T_w/T_{t0} near 0.44 (see Table 1).

Probes

Radial surveys were made across the flow with a pitot, a static pressure, and a thermocouple probe at the axial locations shown in Fig. 2. The 0.11 cm o.d. pitot tube had a flattened tip, either 0.013 or 0.015 cm high, with a 0.005 cm high opening. The 0.10 cm o.d. aspirating thermocouple probe had a flattened tip which was 0.025 cm high. The 0.051 cm o.d. static pressure probe had 0.020 cm diam holes on both sides at a distance of 15 probe diameters from the blunted conical tip. These probes were inserted in a cooled ring, 3.8 cm long, that was moved from one axial location to another from test to test at the same operating condition. The static pressure and thermocouple probes were located 45° circumferentially on either side of the pitot probe. With the probes resting on the surface, the distance from the center of the probes to the surface as well as their orientation relative to the surface were determined visually using a 64-power telescope with a lens scale.

The probes were moved normal to the surface by a micrometer lead screw. The surface location was determined by electrical contact, and the relative probe location was determined with a helipot. A differential pressure transducer was used to measure the difference between the pitot pressure and either a wall static pressure tap when the probe was near the wall, or the atmospheric pressure for the remainder of the traverse. A transducer was also used to measure pressure differences between the static pressure probe and a wall static pressure tap. For both probes, damped time fluctuations of ±1 cm of water were typical. The output signals of the transducers and thermocouple were plotted versus distance from the surface at much finer increments than the points presented herein.

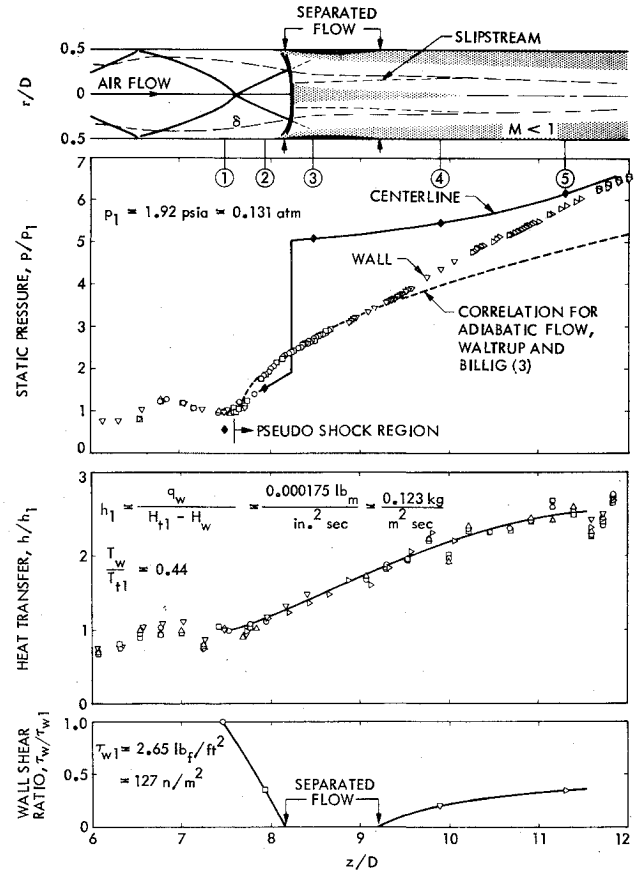

Fig. 2 Pseudo-shock region.

Probe Measurements

Some comments are in order with regard to the accuracy of the probe measurements. The pitot tube was inclined at an angle of between 5° and 10° toward the wall to ensure that the tip touched the wall. The effect of yaw on pitot tubes[5,6] should be negligible up to about 15°. The streamlines (Fig. 3) deduced from the integrated probe measurements indicated that this condition was not exceeded at any of the probe locations. The interaction of the relatively weak oblique shock wave at positions 1 and 2 (Fig. 2) with the pitot bow shock should have influenced the pitot tube reading only at distances less than one tip height from the oblique shock wave.[7] Therefore, the pitot tube measurements (Fig. 4) were good indicators of the shock wave at the positions indicated.

The static pressure probe was designed to allow the local static pressure to recover to within about 2% of the local static pressure upstream of the bow shock wave[8] for a uniform flow. In the axial pressure gradient region good agreement was observed between the extrapolation of the probe measurements to the wall and the wall static pressure measurements (solid points on Fig. 5) opposite the static pressure holes on the probe, not its tip. This axial location for the static pressure measurements was used across the flow. Moreover, the static pressure probe is expected to be sensitive to yaw, unlike the pitot probe. The streamlines in Fig. 3,

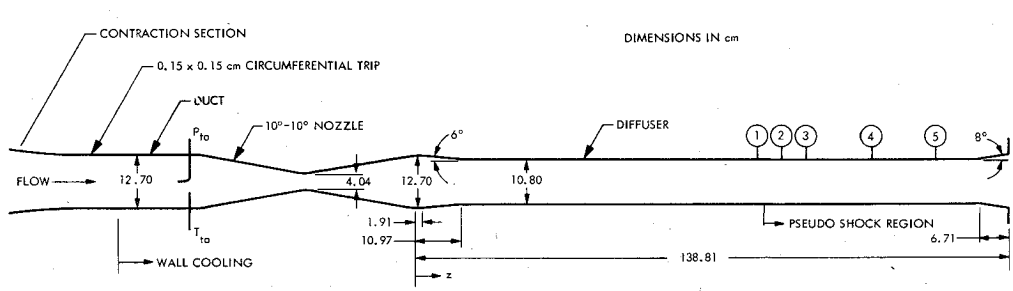

Fig. 1 Test system schematic.

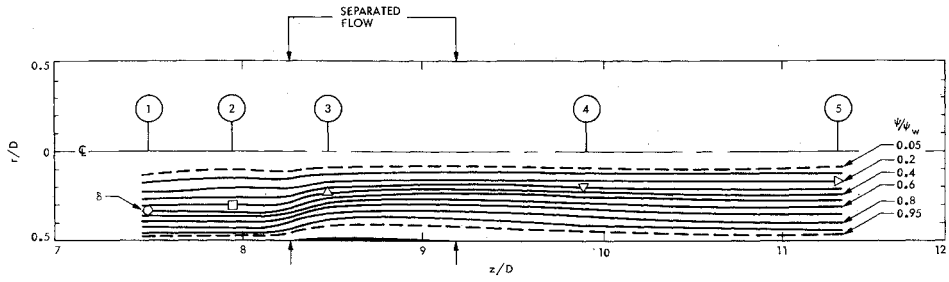

Fig. 3 Streamlines in pseudo-shock region.

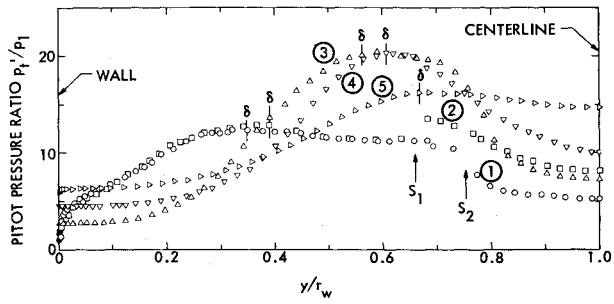

Fig. 4 Pitot pressure profiles.

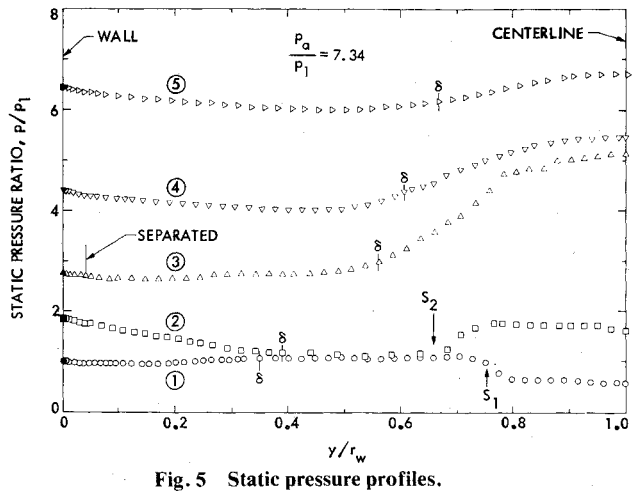

Fig. 5 Static pressure profiles.

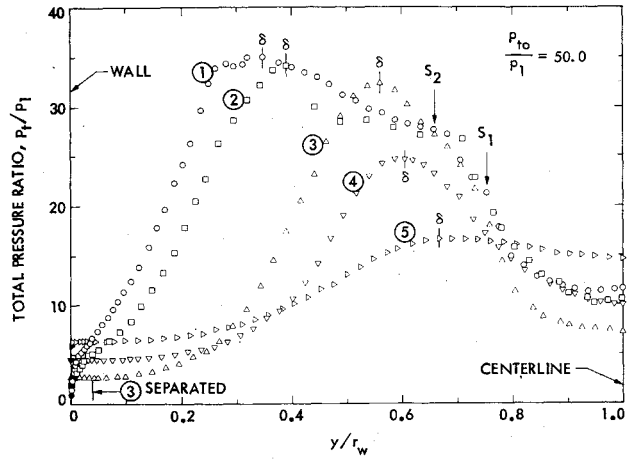

Fig. 6 Total pressure profiles.

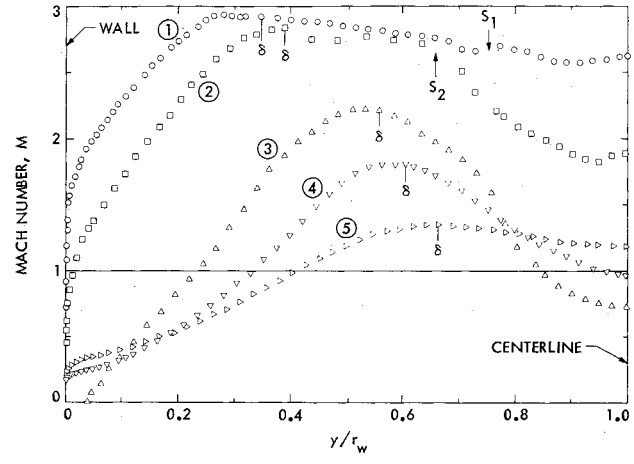

Fig. 7 Mach number profiles, $\gamma = 1.4$.

however, indicate that the flow was nearly parallel to the wall (and therefore the probe) except at position 3 where the flow inclination probably influenced the static pressure probe readings to some degree. Although these streamlines were obtained using the static pressure measurements, substantial changes in the static pressures would be required to significantly alter the flow angles indicated. Another check of the internal consistency of these measurements is the comparison of the derived flow quantities, e.g., the total pressure, axially along each of the streamlines. The variations observed along streamlines using the internal static pressure measurements are understandable, while taking the static pressure to be invariable across the flow at the wall walue. for example, produces physically unacceptable variations. Therefore, these measurements were considered to be sufficiently accurate for the determination of the flowfield described herein.

Table 1 Values of α, β, and $St(c_f/2)$

Position	z, cm	T_w/T_{t0}	α	β	$St/c_f/2)$
1	80.76	.428	.00126	−.042	1.15
2	85.77	.436	.00026	−.061	3.8
3	91.46	.416	—	—	—
4	106.85	.445	.00006	−.090	9.2
5	121.95	.457	.00007	−.072	5.5

The weak oblique shock waves encountered at positions 1 and 2 are expected to influence the static pressure readings when the shock waves intersect the probe either anywhere upstream of the static holes, or within a few probe diameters downstream thereof.[9,10] Because of this interference, a gradual static pressure change (Fig. 5) was observed at each of the shock locations instead of the more abrupt change indicated with the pitot tube (Fig. 4). The total pressures (Fig. 6) and Mach numbers (Fig. 7) obtained from both of these measurements also indicate more gradual changes at these shock locations than probably occurred.

The recovery factor for the temperature probe was determined by comparing its readings in the core flow region with the measured upstream stagnation temperature ($T_{t0} = T_{t1}$). An average recovery factor of 0.92 was used throughout the flow, even in subsonic regions since errors so introduced were relatively small. The thermocouple readings were extrapolated toward the wall to the location of the smaller pitot probe. The temperature gradient at the wall determined from the wall temperature and heat flux measurements was used as a guide

for this extrapolation. Errors associated with the extrapolation are expected to be small, especially for the velocity distribution since it depends upon the square root of the static temperature.

Wall Measurements

The cooled system was instrumented to measure the heat flux, temperature, and static pressure along the wall. Throughout the diffuser throat section, most of the circumferential coolant passages for the heat flux measurements were 2.5 cm wide, although the small cooled rings contained passages of other widths. The wall heat flux for each circumferential passage was determined from the measured water mass flow rate, water temperature rise, and passage gas-side surface area. Most of the passages contained water-side wall thermocouples; when not measured, this temperature was obtained from the average bulk water temperature and the passage heat flux by using conventional heat-transfer relations for channel flow. The gas-side surface temperature T_w was determined from the heat conduction equation. Heat transfer coefficients were obtained from

$$h = \frac{q_w}{(H_{t1} - H_w)}$$

Wall static pressure taps (0.051 cm diam) were located between most of the coolant passages with alternate taps in lone 180° apart. To obtain more detail, a ring was constructed containing numerous closely spaced wall static pressure taps that spiraled around the circumference of the diffuser. This ring was moved between tests to obtain data at several locations along the diffuser. Differences between the wall static pressure and atmospheric pressure were measured with transducers. Figure 2 indicates reasonably good test to test agreement.

Results

The interpretation of the flowfield presented is based on an understanding of the axial changes of quantities along the streamlines (Fig. 3) obtained from the radial traverses across the flow. The pitot (Fig. 4) and static (Fig. 5) pressure readings locally were used to evaluate the total pressure (Fig. 6) and Mach number (Fig. 7). The local temperature (Fig. 8) was obtained from the thermocouple readings based on the recovery factor and the local Mach number. The velocity profiles relative to the value at δ are shown in the wall boundary-layer region in Fig. 9. For completeness, the mass flux profiles that were integrated to obtain the streamlines in Fig. 3 are shown in Fig. 10.

The pseudo-shock region began just downstream of probe position 1 as indicated by the continuous rise in both the wall static pressure and heat-transfer coefficient shown in Fig. 2. The oblique shock wave generated at the diffuser inlet underwent multiple reflections from the centerline and the boundary layer along the wall before terminating at the beginning of the pseudo-shock region. In these upstream weak oblique shock wave interactions, the wall static pressure and heat-transfer increase at the shock impingement location, and subsequently decrease in the acceleration region between the compressive shocks as is required to maintain the mass balance for the flow through the diffuser. The pitot tube traverses at positions 1 and 2 determined the location of the shock reflection from the centerline. As mentioned previously, the static pressure probe indicated a gradual change in static pressure near the shock location at positions 1 and 2 (Fig. 5) and also indicated that the effect of this oblique shock may have continued to position 3 near $y/r_w = 0.26$ (also see Fig. 2) where rapid changes in boundary-layer development and nearly sonic Mach numbers prevented detection with the pitot tube.

The flow was divided into boundary layer and core flow regions at the radial maximum of the total pressure δ (see Fig. 6). The variation of the boundary-layer thickness δ so obtained in the pseudo shock region is shown in Fig. 2 by the

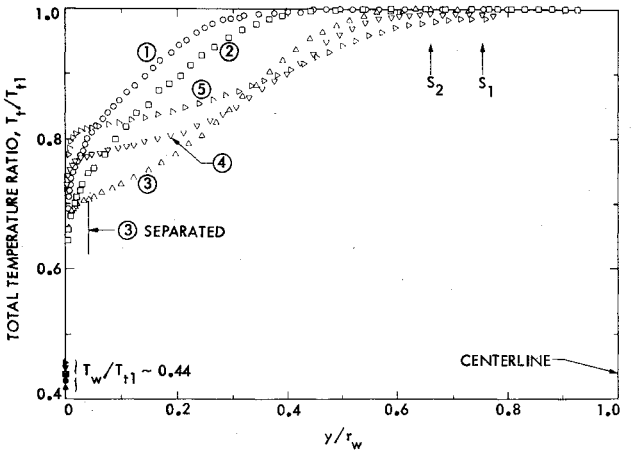

Fig. 8 Total temperature profiles.

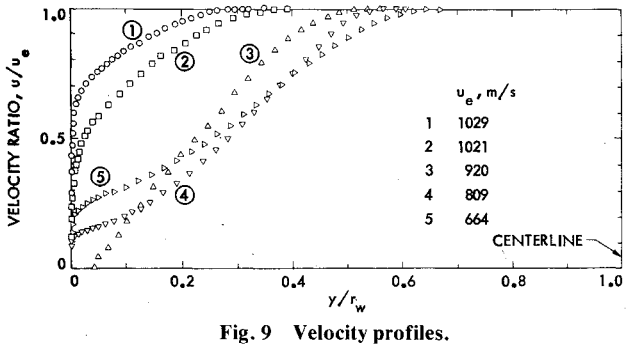

Fig. 9 Velocity profiles.

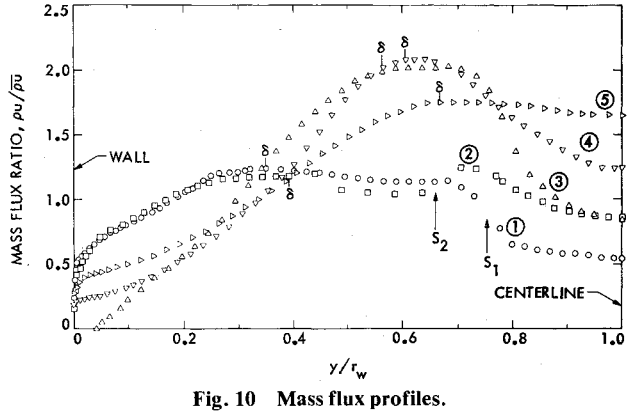

Fig. 10 Mass flux profiles.

dashed line. The thermal boundary-layer thickness Δ (Fig. 8) is seen to be larger than δ at all probe locations (compare Fig. 9 with Fig. 8).

At probe position 1 the boundary layer was determined to be turbulent by its structure in the wall region as discussed subsequently. By terminating the boundary-layer integrations at δ, the upstream momentum, displacement, and energy thicknesses were $\theta_1 = 0.11$ cm, $\delta_1^* = 0.40$ cm, and $\phi_1 = 0.17$ cm, respectively. At the edge of the velocity boundary layer $\delta_1 = 1.88$ cm, the Mach number was 2.92, the unit Reynolds number $\rho_e u_e/\mu_e$ was 88,700 cm^{-1}, and the total pressure was 4.56 atm. The static pressure increased slightly in the outer portion of the boundary layer (Fig. 5) and was fairly constant in the core flow region except for the smeared change across the weak oblique shock. In spite of the large change in the total pressure radially across the core flow (Fig. 6) the Mach number varied only between 2.9 and 2.6 (Fig. 7).

Probe position 2 was in the pseudo-shock region as indicated by the static pressure increase along the wall upstream. This pressure rise over that at position 1 originated near the wall and progressively extended into the flow (Fig. 5)

causing a thickening of the boundary layer. With the streamlines remaining reasonably parallel to the wall (note agreement of the mass flux distributions in Fig. 10), the flow through the bulk of the boundary layer was decelerated, thereby causing a decrease in the Mach number, total pressure, and velocity. The streamlines were obtained by integrating the axial mass flux distribution radially outward from the centerline

$$\Psi = \int_0^r \rho u r dr$$

and then normalized by the measured flow through the diffuser. The core flow region at probe position 2 apparently had not been affected by the onset of the pseudo-shock region. The oblique shock reflected off the centerline, slightly dropping the total pressure in the core flow, causing a noticeable increase in static pressure, and resulting in a decrease in Mach number.

The measurements at probe position 3 revealed an extensive subsonic region in the center of the core flow (Fig. 7), thus indicating that a strong shock wave was located between probe positions 2 and 3. A reasonable estimate was made of the location of this shock which was normal to the flow at the centerline (Fig. 2) by extrapolation of downstream and upstream conditions (Mach number and static and pitot pressures). The measurements at probe position 3 also revealed a separated flow region near the wall (Fig. 9). The beginning of the separated flow region was established by bleeding a small amount of ammonia gas through the wall static pressure taps and observing the embedded flow patterns in a thin film of ammonia-sensitive Diazo paint on the surface. The compressive turning of the flow radially inward beyond the separated flow region generated the Mach-disk-like shock wave near the centerline. This turning of the flow is evident in Fig. 3 where the streamlines are shown. The estimated wall shear stress rapidly decreased and extrapolated to zero at the separation location. Aside from the weak oblique shock wave that may have penetrated through the strong shock to probe position 3, there was no evidence of other shock waves in the flow at probe position 3, nor at subsequent downstream probe locations 4 and 5.

The static pressure between probe positions 2 and 3 increased substantially all across the flow (Fig. 5). The streamlines indicated that the flow was displaced to some extent by the separation region toward the centerline (Fig. 3). The gas located radially beyond the separated flow region, being shielded from the cooled wall by the separation region itself, was heated by the higher total temperature outer gas flow (Fig. 8). The bulk of the drop in total temperature between probe positions 2 and 3 at a given radial location was the result of the displacement of streamlines, and not due to a change in total temperature along streamlines. The thickness of the separation region at probe position 3 was relatively small, being about 4% of the diffuser radius r_w. Flow reattachment, determined by the previously mentioned visualization technique, occurred downstream of probe position 3 as indicated in Fig. 2. The axial extent of the separation region was one diffuser diameter.

The subsonic flow region downstream of the normal shock disappeared as the core flow accelerated to supersonic speeds. The divergent outer edge of the viscous slipstream extended into the boundary layer, forming a totally viscous flow in the vicinity of probe position 4.

Analysis of the measurements (see Figs. 4-8 and 10) revealed that as the flow progressed from probe position 3 to position 5 the radial variations across the flow decreased, and the static pressure increased along the streamlines. The total pressure, however, increased along the convergent streamlines in the core flow region near the centerline and throughout most of the subsonic flow region near the wall (Fig. 6). In the large annular region between the core flow and wall region the total pressure decreased along the divergent streamlines between probe positions 3 and 5. Correspondingly, the Mach number (Fig. 7) and mass flux (Fig. 10) increased in the core flow and wall regions with axial distance, while they decreased in the annular region. Near the wall, the radial total temperature gradients were much larger at probe positions 4 and 5 than at positions 1 and 2 (Fig. 8).

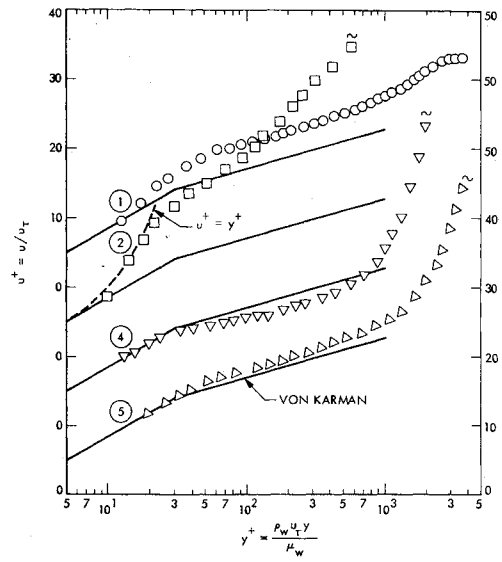

Fig. 11 Velocity profiles, u^+ vs y^+.

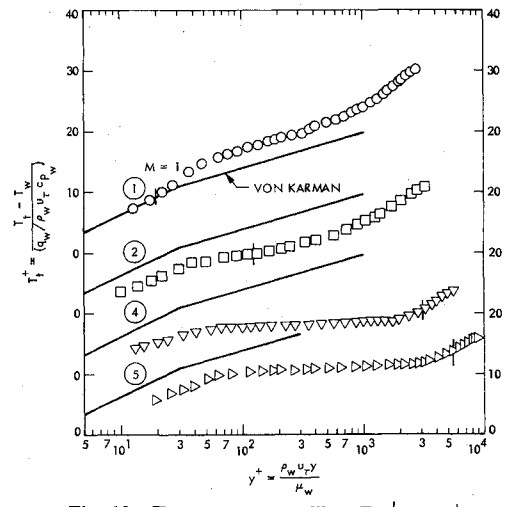

Fig. 12 Temperature profiles, $T_t{}^+$ vs y^+.

The attached boundary-layer profiles are shown in Figs. 11 and 12 in terms of u^+, T_t^+ and y^+. The wall shear stress in terms of the friction velocity $u_\tau = (\tau_w/\rho_w)^{1/2}$ was determined to provide a reasonable fit of the data to the von Karman reference curve in the viscous sublayer. At probe position 2, better agreement was found with the laminar sublayer relation $u^+ = y^+$ which was used instead. Large wake components are evident in the adverse pressure gradient region at probe positions 2, 4, and 5, while at the upstream position 1, the data lie above the von Karman curve beyond the viscous sublayer similar to that observed previously with wall cooling.[11, 12] Values of the heat-transfer parameter β and frictional heating parameter [12] α are tabulated in Table 1.

The temperature profiles shown in Fig. 12 indicate a large difference between the data in the adverse pressure gradient region at probe positions 2, 4, and 5 and at the upstream position 1. Upstream, the data beyond the viscous sublayer lie above the von Karman profile shown as a reference curve, while downstream, the temperature profiles were well below the von Karman profile. This latter trend has also been observed in low speed, essentially constant property turbulent

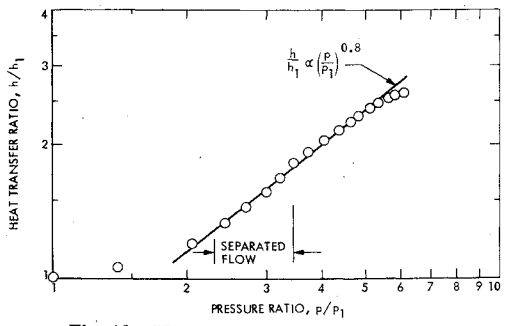

Fig. 13 Heat transfer-pressure relationship.

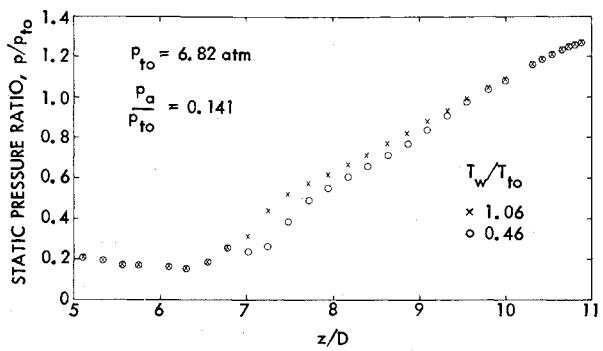

Fig. 14 Wall static pressure distributions with and without surface cooling.

boundary layers in adverse pressure gradient regions.[13] Since the thermal resistance is proportional to T_t^+ at the edge of the layer, the profiles in the adverse pressure gradient region indicated lower thermal resistances and thus higher heat transfer than inferred from the von Karman form of Reynolds analogy, as well as other forms such as the Colburn relation. Values of the Stanton number-friction coefficient group $St/(c_f/2)$ were relatively large in the pseudo-shock region (Table 1). Of note is that the maximum values of T_t^+ in the flow were 2 to 4% greater than the values shown in Fig. 12 furthest from the wall.

The measured heat-transfer coefficient in the pseudo-shock region increased by a factor of 2.6 (Fig. 2) over the upstream value. In the region of the upstream weak oblique shock wave reflection the rise was much less. The heat-transfer coefficient ratio in the pseudo-shock region varied approximately as the 0.8 power of the wall static pressure ratio over most of the pseudo-shock region (Fig. 13). This power law dependence is essentially the same as for single shock wave-turbulent boundary-layer interactions (e.g., see Ref. 14) as also was the case for the upstream single wave interaction herein.

In the pseudo-shock region after reattachment, the estimated wall shear stress increased, but was still considerably less than the upstream value (Fig. 2). The empirical correlation of the wall pressure rise given in Ref. 3 for an adiabatic wall and flow separation along the entire wall underestimates the measured pressure rise with wall cooling (Fig. 2) downstream of reattachment as one might expect because of the different flow structure. In this connection it should be noted that wall measurements (but not internal flow measurements) were made at a stagnation pressure of $p_{t0} = 6.82$ atm both with a small amount of surface heating ($T_w/T_{t0} \cong 1.06$) and with surface cooling ($T_w/T_{t0} \cong 0.46$). For the set of measurements shown in Figure 14, the cooled rings had been removed so that the diffuser throat was 9.9 throat diameters long. The various features of these profiles are similar to that shown in Fig. 2 for which internal flow measurements were made at a slightly lower stagnation pressure. All three wall static pressure distributions indicate a slight increase in slope at $p/p_{t0} \cong 0.07$ ($p/p_1 \cong 3.5$ on Fig. 2) where the measured flow with wall cooling reattached. Furthermore, this behavior is not typical of the correlation by Waltrup and Billig[3] for flows which remained separated along the entire diffusers with adiabatic walls. Therefore, it is believed that the flows investigated herein separated and reattached in the pseudo-shock region for the slight heating case as well as for the wall cooling case. The thermal condition of the wall, however, did change the length of the pseudo-shock region slightly, as evident in Fig. 14.

Summary

The present measurements have revealed the complex flowfield in a pseudo-shock region with surface cooling. This strong compression in the supersonic diffuser was predominantly a viscous process. Only one Mach-disk-like shock wave emanated from the beginning of the embedded separated flow region near the start of the pseudo-shock region. The boundary layer reattached one diam downstream, so that over most of the pseudo-shock region the flow was not separated. The thick subsonic flow region formed in the separation process continued to grow downstream. The flow accelerated in regions along the wall and near the centerline. The latter resulted in the disappearance of the embedded subsonic flow region downstream of the Mach-disk-like shock. The bulk of the flow, however, decelerated in an annular region between these two accelerating flow regions. Except in a small region very close to the wall where shear stresses and heat transfer predominate, radial gradients diminished along the flow.

The wall static pressure increase along the flow originated near the wall and extended into the flow. The compressive turning of the flow radially inward in the beginning of the pressure rise region where the flow separated generated the Mach-disk-like shock wave near the centerline. An empirical correlation[3] of the wall pressure rise for adiabatic flows that remained separated underestimated the data with wall cooling downstream of reattachment. From our wall measurements made with a small amount of surface heating, it was inferred that there was no significant difference in the flow structure with and without surface cooling, i.e., flow reattachment occurred downstream of separation in the system.

In the separated and reattached flow regions, the heat-transfer coefficient varied approximately as the 0.8 power of the wall static pressure. In the reattached region the von Karman form of Reynolds analogy or the Colburn relation considerably underestimated the heat-transfer-friction relationship as one might expect because of the adverse pressure gradient and flow redevelopment. In the reattachment region the estimated wall shear stress increased, but was still considerably less than upstream of flow separation.

References

[1] Massier, P. F. and Roschke, E. J., "Experimental Investigation of Exhaust Diffusers for Rocket Engines," *Progress in Astronautics and Rocketry,* Vol. 2, Liquid Rockets and Propellants, Academic Press, N.Y., 1960, pp. 3-75.

[2] Crocco, L., "One-Dimensional Treatment of Steady Gas Dynamics," *Fundamentals of Gas Dynamics,* Vol. III, Edited by H. W. Emmons, Princeton University Press, Princeton, N. J., 1958, p. 115.

[3] Waltrup, P. J. and Billig, F. S., "Structure of Shock Waves in Cylindrical Ducts," *AIAA Journal,* Vol. 11, Oct. 1973, pp. 1404-1408.

[4] Waltrup, P. J. and Cameron, J. M., "Wall Shear and Boundary-Layer Measurements in Shock Separated Flow," *AIAA Journal,* Vol. 12, June 1974, pp. 878-880.

[5] Gracey, W., Lerko, W., and Russel, W. B., "Wind-Tunnel Investigation of a Number of Total-Pressure Tubes at High Angles of Attack. Subsonic Speeds," NACA Tech. Note 2331, 1951.

[6] Becker, H. A., and Brown, A. P. G., "Response of Pitot Probes in Turbulent Streams," *Journal of Fluid Mechanics,* Vol. 62, Pt. 1, 1974, pp. 85-114.

[7] Bannink, W. J. and Nebbeling, C., "Determination of the Position of a Shock Wave from Pitot Tube Experiments," *AIAA Journal,* Vol. 7, April 1969, pp. 796-797.

[8]Cronvich, L. L., "Pressure Distributions Over a Cylinder with Conical or Hemispherical Head at Supersonic Velocities," Rpt. CM-528, Applied Physics Laboratory, Johns Hopkins University, Silver Spring, Md., Feb., 1949. (Also see Shapiro, A. H., "The Dynamics and Thermodynamics of Compressible Fluid Flow," Vol. II, The Ronald Press Co., N. Y., 1954, pp. 696-697.)

[9]Back, L.H. and Cuffel, R.F., "Static Pressure Measurements Near an Oblique Shock Wave," *AIAA Journal,* Vol. 9, Feb. 1971, pp. 345-347.

[10]Rode, J. E. and Skoglund, V. J., "A Static Pressure Probe for the Interaction Region of a Shock Wave and Boundary Layer," *Journal of Aeronautical Science,* Vol. 29, Oct. 1962, pp. 1262-1263.

[11]Back, L. H. and Cuffel, R. F., "Shock Wave-Turbulent Boundary Layer Interactions with and without Surface Cooling," *AIAA Journal,* Vol. 14, April 1976, pp. 526-532.

[12]Back, L. H. and Cuffel, R. F., "Turbulent Boundary Layer and Heat Transfer Measurements along a Convergent-Divergent Nozzle," ASME *Journal of Heat Transfer,* Ser. C, Vol. 93, No. 4, Nov. 1971, pp. 397-407.

[13]Perry, A. E., Bell, J. B., and Joubert, P. N., "Velocity and Temperature Profiles in Adverse Pressure Gradient Turbulent Boundary Layers," *Journal of Fluid Mechanics,* Vol. 25, Pt. 2, 1966, pp. 299-320.

[14]Back, L. H. and Cuffel, R. F., "Changes in Heat Transfer from Turbulent Boundary Layers Interacting with Shock Waves and Expansion Waves," *AIAA Journal,* Vol. 8, Oct. 1970, pp. 1871-1873.